

Stress scale factor and critical plane models under multiaxial proportional loading histories



Manuel de Freitas^{a,*}, Luis Reis^a, Marco Antonio Meggiolaro^b, Jaime Tupiassú Pinho de Castro^b

^a IDMEC, Instituto Superior Técnico, Universidade de Lisboa, Av. Rovisco Pais, 1049-001 Lisboa, Portugal

^b Pontifical Catholic University of Rio de Janeiro, PUC-Rio, Rua Marquês de São Vicente 225, Rio de Janeiro, RJ 22451-900, Brazil

ARTICLE INFO

Article history:

Received 15 September 2016

Received in revised form 16 December 2016

Accepted 17 December 2016

Available online 24 December 2016

Keywords:

Multiaxial fatigue

Damage calculation

Stress scale factor

Critical-plane approach

ABSTRACT

It has been experimentally proven that the shear stress level needed to cause fatigue failure is lower than the axial one. This fact has led to consider a Stress Scale Factor (SSF) between shear and axial stress to reduce different applied stresses to the same shear stress space or principal stress space, consequently facilitating the yielding analysis or fatigue damage evaluations. Most of multiaxial fatigue models use an SSF, and materials can be classified as shear sensitive (low SSF values) or tensile sensitive (large SSF values), depending on the main fatigue microcrack initiation process under multiaxial loadings. The use of SSF is quite common in many multiaxial fatigue criteria based on the critical plane approach. Such criteria adopt a SSF value assumed constant for a given material, sometimes varying with the fatigue life (in cycles) but not with the SAR (Stress Amplitude Ratio), the stress amplitude level, or the loading path shape. In this work, in-phase proportional tension-torsion tests related to 42CrMo4 steel specimens for several values of SAR are presented. The SSF approach is then compared with critical-plane models, based on their predicted fatigue lives and the observed ones for the studied tension-torsion histories.

© 2016 Elsevier Ltd. All rights reserved.

1. Introduction

Experimentally, it has been proven that the shear stress level needed to cause fatigue failure is lower than the axial one and several references can be found in the literature related to this material behavior [1,2]. This fact has led to consider a Stress Scale Factor (SSF) between shear and axial stress in order to reduce different applied stresses to the same shear stress space or principal stress space to facilitate the yielding analysis or fatigue damage evaluations. In this way, most of multiaxial fatigue models use a stress scale factor to consider the fatigue damage contributions from the axial and shear stress components regarding the material strength degradation.

Materials can be classified as shear or tensile sensitive, depending on the main fatigue microcrack initiation process under multiaxial loadings [2]. Initiating microcracks under multiaxial loading are usually sub-divided into shear or tensile types. The dominant fatigue mechanism in so-called shear-sensitive materials is Mode II and microcracks nucleate along a shear plane where the range of the shear components is maximum, with the normal components only playing a secondary role. However, other materials such as 304 stainless steel under certain load histories, and cast irons [1], may initiate fatigue cracks in plane of maximum tensile strain or stress ranges, in this case, even if the microcrack nucleates in shear, its so-

* Corresponding author.

E-mail addresses: mfreitas@dem.ist.utl.pt (M. de Freitas), luis.g.reis@ist.utl.pt (L. Reis), meggi@puc-rio.br (M.A. Meggiolaro), jtcastro@puc-rio.br (J.T.P. de Castro).

Nomenclature

ESWT	elastic Smith Watson Topper
SAR	stress amplitude ratio
SSF	stress scale factor
A, b	power law fitting parameters of SN curve
a, b, c, d, f, g, h, i	material constants of SSF function
E	Young's modulus
N	number of cycles
R	stress ratio
S_L	axial or bending fatigue limit
S_{Lp}	pulsated axial fatigue limit
α_F	Findley's coefficient
α_C	Crossland's coefficient
β_F	Findley's damage parameter
β_C	Crossland's damage parameter
ε	strain
γ	shear strain
λ	stress amplitude ratio
θ	angle of critical plane
σ_α	axial stress amplitude
$\sigma_c, \varepsilon_c, b, c$	Coffin-Manson's material parameters
τ_α	torsional stress amplitude
τ_L	torsional fatigue limit
τ_c, b_τ	torsional strength coefficient and exponent

called initiation life (which always includes some microcrack propagation) is controlled by its growth in a direction perpendicular to the maximum principal stress or strain. Moreover, a material can be shear-sensitive for short fatigue life, but tensile-sensitive for long fatigue life, a behavior that can also depend on the loading type.

The shear or tensile nature of the initiating microcrack can be evaluated from a stress scale factor (SSF): low values of the SSF indicate a shear-sensitive material, which usually requires shear-based damage models such as Findley's [3] or Fatemi-Socie's [4], while a large SSF indicates that a tensile-based model should be used, like Smith-Watson-Topper's [5].

The approach proposed by Anes et al. [6], for tension-torsion histories, combines the shear and normal stress amplitudes applied on the specimen cross section, using a SSF polynomial function that depends on the Stress Amplitude Ratio (SAR) between shear and normal components. Such an approach has been successfully applied to multiaxial fatigue life predictions either under constant amplitude loading or under variable amplitude loading [7,8]. The present method is considered as an alternative to multiaxial fatigue life prediction by means of critical plane-based criteria, employed for both constant [9–12] and variable amplitude loadings [13–15]. The critical plane approach calculates the damage on the plane where damage is maximized (not on the plane where the load is applied) while adopting a SSF value that is assumed constant for a given material, sometimes varying with the fatigue life (in cycles), but not with the SAR, the stress amplitude level, or the loading path shape.

In this work, in-phase proportional tension-torsion experiments that were carried out in previous studies [6–8] on 42CrMo4 steel round specimens for several values of the SAR are re-analyzed in terms of SSF and critical plane methods. The SSF approach in [6] is then compared with two critical plane methods in [3,4], based on their predicted fatigue lives and the observed values for the examined tension-torsion histories.

2. The SSF method

The SSF parameter presented for each criterion is obtained in tension-compression, bending or pure shear loading conditions. This approach conducts to results where the tension-compression or bending S-N curves can be directly related to the pure shear data or vice versa. The main statement is that the multiaxial model must also explain the uniaxial results; however, the combined effect between axial and shear components is based on the uniaxial fatigue data, missing the combined damage effect. The SSF method based on an equivalent shear stress approach, proposed in [6], considers that both the SAR and the stress loading level significantly influence the material fatigue strength. Such effects are accounted for through the SSF function, which transforms an axial damage into a shear one. With this equivalent stress, it is also possible to estimate fatigue lives N_f using the uniaxial shear stress S-N curve represented as

$$\max_{\text{block}}(\tau + \text{ssf} \cdot \sigma) = A(N_f)^b \quad (1)$$

where A and b are respectively the coefficient and exponent of the S-N curve, and

$$\text{ssf}(\sigma_a, \lambda) = a + b \cdot \sigma_a + c \cdot \sigma_a^2 + d \cdot \sigma_a^3 + f \cdot \lambda^2 + g \cdot \lambda^3 + h \cdot \lambda^4 + i \cdot \lambda^5 \quad (2)$$

where $\lambda \equiv \tan^{-1}(\tau_a/\sigma_a)$ is the SAR and σ_a and τ_a are respectively the amplitude of the axial and shear component of the tension-torsion loading. The constants from “a” to “i” are determined through experimental tests and, therefore, the SSF function is a material fatigue property.

3. Critical plane approach

The critical-plane approach assumes that fatigue life can be calculated from the damage on the critical plane at the critical point [16,17]. It also assumes that damage on all other planes do not influence the initiation of the microcrack. Here, the main calculation challenge is to compute the accumulated damage in many candidate planes at the critical point, to find the direction of the critical one where the damage is maximized (and thus where the crack is expected to initiate). This search is very much simplified for in-phase proportional constant amplitude load histories, such as the ones studied in this work.

3.1. Candidate planes for crack initiation

For materials that tend to initiate a single dominant microcrack (a typical fatigue behavior observed in most metallic alloys), Bannantine and Socie [18] narrowed down the search space for the critical plane. They classified the most common initial cracks into three types, which depend on the fatigue damage mechanism: (1) Case A tensile or (2) Case A shear cracks, which grow in planes perpendicular to the free surface, or (3) Case B shear cracks, which grow in planes that form an angle equal to 45° with the surface.

The initiation of a Case A microcrack, which grow along a critical plane *perpendicular* to the free surface, is controlled by the combination of its four projected stresses and strains:

$$\begin{aligned} \tau_A(\theta) &= \tau'_{xy}(\theta) = \tau_{xy} \cos 2\theta + 0.5 \cdot (\sigma_y - \sigma_x) \cdot \sin 2\theta \\ \sigma_{\perp}(\theta) &= \sigma'_x(\theta) = \sigma_x \cdot \cos^2 \theta + \sigma_y \cdot \sin^2 \theta + \tau_{xy} \sin 2\theta \\ \gamma_A(\theta) &= \gamma_{xy} \cos 2\theta + (\varepsilon_y - \varepsilon_x) \cdot \sin 2\theta \\ \varepsilon_{\perp}(\theta) &= \varepsilon_x \cdot \cos^2 \theta + \varepsilon_y \cdot \sin^2 \theta + 0.5 \cdot \gamma_{xy} \sin 2\theta \end{aligned} \quad (3)$$

where θ is the angle of the plane as shown in Fig. 1, σ_x , σ_y , τ_{xy} , ε_x , ε_y and γ_{xy} are time-varying components defined by the load history. Fig. 1 shows the stress states and Mohr circles associated with such Case A cracks.

For a proportional loading history (σ_x , τ_{xy}) (with amplitudes $\sigma_a \geq 0$ and $\tau_a \geq 0$), the projected stresses during the peak load (σ_a , τ_a) are given by:

$$\begin{aligned} \tau_{\text{Apeak}}(\theta) &= \tau_a \cos 2\theta - 0.5 \cdot \sigma_a \cdot \sin 2\theta \\ \sigma_{\perp\text{peak}}(\theta) &= \sigma_a \cdot \cos^2 \theta + \tau_a \sin 2\theta \end{aligned} \quad (4)$$

and the projected stresses during the valley ($-\sigma_a$, $-\tau_a$) are:

$$\begin{aligned} \tau_{\text{Avalley}}(\theta) &= -\tau_a \cos 2\theta + 0.5 \cdot \sigma_a \cdot \sin 2\theta \\ \sigma_{\perp\text{valley}}(\theta) &= -\sigma_a \cdot \cos^2 \theta - \tau_a \sin 2\theta \end{aligned} \quad (5)$$

From these stresses at each peak and valley of the loading history, the projected shear stress amplitude for each Case A candidate plane with angle θ can be computed:

$$\frac{\Delta\tau_A(\theta)}{2} = \frac{|\tau_{\text{Apeak}}(\theta) - \tau_{\text{Avalley}}(\theta)|}{2} = |\tau_a \cos 2\theta - 0.5 \cdot \sigma_a \cdot \sin 2\theta| \quad (6)$$

and the projected normal stress amplitude is:

$$\frac{\Delta\sigma_{\perp}(\theta)}{2} = \frac{|\sigma_{\perp\text{peak}}(\theta) - \sigma_{\perp\text{valley}}(\theta)|}{2} = |\sigma_a \cdot \cos^2 \theta + \tau_a \sin 2\theta| \quad (7)$$

Further, the maximum projected stress is given by:

$$\sigma_{\perp\text{max}}(\theta) = \max\{\sigma_{\perp\text{peak}}(\theta), \sigma_{\perp\text{valley}}(\theta)\} = |\sigma_a \cdot \cos^2 \theta + \tau_a \sin 2\theta| \quad (8)$$

Note that the maximum projected stress could be $\sigma_{\perp\text{valley}}(\theta)$ for $\sin 2\theta < 0$ and large τ_a . Therefore the above absolute value functions are required to guarantee tensile maximum stresses in this fully-alternate example. Moreover, due to symmetry, the mean normal stress $\sigma_{\perp\text{m}}(\theta)$ is equal to zero.

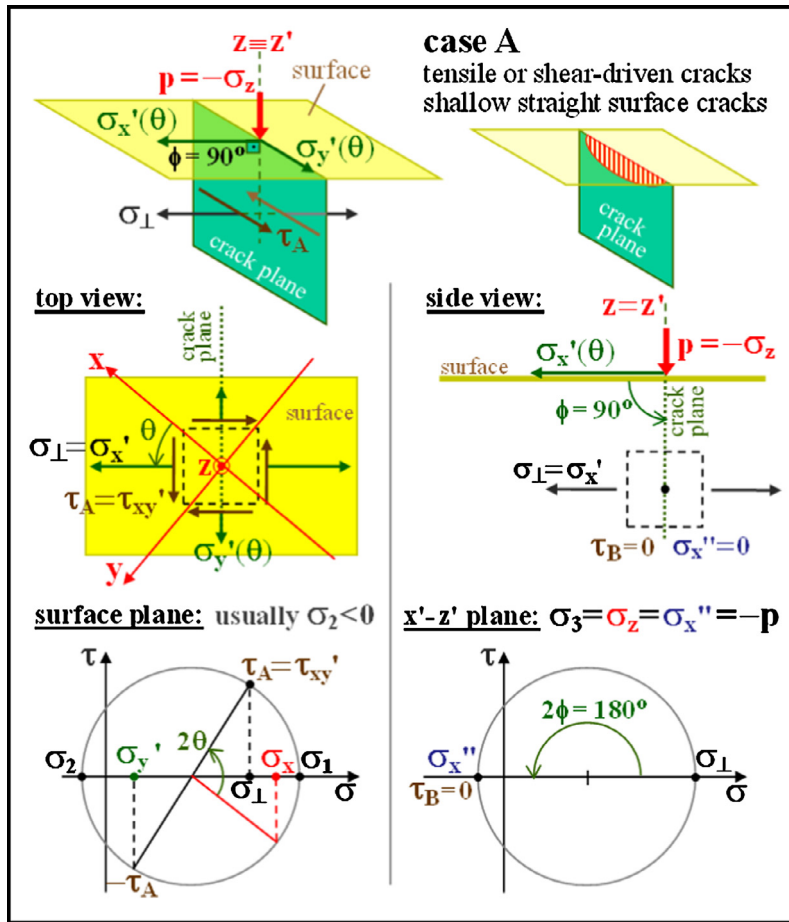


Fig. 1. Stress states and Mohr's circles for the initiation of a Case A microcrack at $(\theta, 90^\circ)$ planes perpendicular to a free-surface, with an optional surface pressure p .

Case B shear cracks, which initiate at 45° from the free surface, is not examined in this work, since they are not likely to initiate in tension-torsion experiments, which have negative biaxiality ratios $\sigma_2/\sigma_1 < 0$, where σ_1 and σ_2 are the principal stresses on the free surface. Case B shear cracks are usually the case of positive biaxiality ratios $\sigma_2/\sigma_1 > 0$, where the microcrack initiation is on the maximum shear plane at 45° from the free surface, controlled by the maximum absolute σ_1 and the free-surface principal stress σ_3 .

3.2. Findley's shear model

Findley explicitly introduced the critical plane idea in 1959 [3], proposing a stress-based fatigue damage model applicable to non-proportional multiaxial loads. His seminal idea was further developed in 1991 by Bannantine and Socie [18], and it is now used in most advanced models for predicting fatigue damage under multiaxial loads in materials that initiate a single dominant crack under low loads, like most metallic alloys. Such models assume that the fatigue crack initiates at the component's critical point on its critical plane, where a suitable damage parameter is maximized. The critical plane approach is physics-based and considers in a reasonable way how the fatigue cracking process works under multiaxial loads in those materials.

Indeed, when the principal directions vary along time, the cracks certainly have a problem to “decide” in which direction they should initiate. However, since all natural processes tend to choose the path of least effort, they probably would like to do so in the direction where the accumulated fatigue damage is maximized. Models based on this idea are thus sensible, but they have a large computational cost, since they need to identify the critical plane direction at the critical point (typically requiring under free surface conditions a search among at least 18 Case A and 18 Case B candidate planes, for a 10° discretization in θ), an additional non-negligible complication in fatigue damage calculations, only viable because of the low cost of powerful computers nowadays.

Findley assumed that the fatigue damage is caused by the parameter $[\Delta\tau/2 + \alpha_F \cdot \sigma_{\perp\max}]$, which combines the shear stress range $\Delta\tau/2$ acting on the critical plane with the peak of the normal stress perpendicular to that plane $\sigma_{\perp\max}$, during the considered load event. In this way, fatigue cracking would take place at the critical point in directions where this reasonable damage parameter is maximized.

Findley's model is shear-based, since its main cyclic damage parameter is the shear range $\Delta\tau$ and not $\Delta\sigma_{\perp}$. Therefore, such model should be used only if nominally elastic amplitudes would initiate Case A or B shear cracks, not Case A tensile cracks.

For a Case A candidate plane, which is perpendicular to the free surface and makes an angle θ with the x axis, it follows that $\Delta\tau/2 \equiv \Delta\tau_A(\theta)/2$ and $\sigma_{\perp\max} \equiv \sigma_{\perp\max}(\theta)$. Therefore, Findley's infinite life criterion (for multiaxial fatigue under any type of loading) for Case A candidate planes is given by the maximization problem

$$\max_{\theta} [\Delta\tau_A(\theta)/2 + \alpha_F \cdot \sigma_{\perp\max}(\theta)] = \beta_F \quad (9)$$

where Findley's coefficient α_F and fatigue limit β_F must be calibrated from measurements in at least two types of fatigue tests, e.g. under rotatory bending and cyclic torsion, or else under push-pull tests at $R = \sigma_{\min}/\sigma_{\max} = 0$ and $R = -1$.

Let's now calibrate the constants α_F and β_F of Findley's shear-based model from the fully-reversed uniaxial fatigue limit $S_L(R = -1)$ and the torsional fatigue limit τ_L measured under pure cyclic torsion. The first step is to find whether fully-reversed uniaxial stresses with amplitudes slightly higher than S_L would induce Case A tensile, Case A shear, or Case B shear cracks. If they induce Case A tensile cracks, then the material is probably tensile-sensitive, and torsional loads are also likely to induce Case A tensile cracks. For tensile-sensitive materials, a different fatigue damage model that includes the effect of $\Delta\sigma_{\perp}$ is discussed in the next section.

Case A and Case B shear cracks require different calibration procedures. Since only the former is considered in this work, calibration is here performed only for the former case. For Case A shear cracks (which are always perpendicular to the free surface) under uniaxial conditions (i.e. shear amplitude $\tau_a = 0$), it follows from Eqs. (6) and (8) that

$$\frac{\Delta\tau_A(\theta)}{2} = |-0.5 \cdot \sigma_a \cdot \sin 2\theta| = 0.5 \cdot \sigma_a |\sin 2\theta| \quad \text{and} \quad \sigma_{\perp\max}(\theta) = |\sigma_a \cdot \cos^2 \theta| = \sigma_a \cdot \cos^2 \theta \quad (10)$$

Findley criterion is then obtained in this uniaxial case from the following maximization problem:

$$\max_{\theta} [\Delta\tau_A(\theta)/2 + \alpha_F \cdot \sigma_{\perp\max}(\theta)] \equiv \max_{\theta} [0.5\sigma_a \cdot |\sin 2\theta| + \alpha_F \cdot \sigma_a \cos^2 \theta] \quad (11)$$

In the search space $0^\circ \leq \theta \leq 90^\circ$ where $|\sin 2\theta| \equiv \sin 2\theta$, this maximization problem is solved for a Case A critical plane whose θ_{cr} is obtained after equating to zero the derivative of the damage parameter with respect to θ :

$$\sigma_a \cos 2\theta - \alpha_F \cdot \sigma_a \underbrace{2 \cos \theta \sin \theta}_{\sin 2\theta} = 0 \Rightarrow \theta = \theta_{cr} = 0.5 \cdot \tan^{-1} \left(\frac{1}{\alpha_F} \right) \quad (\text{Case A, uniaxial case}) \quad (12)$$

Replacing this θ_{cr} solution into Findley's Eq. (9), it becomes

$$0.5 \cdot \sigma_a \cdot \left(\sqrt{1 + \alpha_F^2} + \alpha_F \right) = \beta_F \quad (\text{Case A, uniaxial case}) \quad (13)$$

The other θ solution of Eq. (11) is within the remaining search space $90^\circ < \theta < 180^\circ$, however the associated candidate plane $\theta = 180^\circ - \theta_{cr}$ results in a lower damage parameter than the one from the θ_{cr} plane, thus it can be ignored.

On the other hand, under pure torsion, i.e. with normal amplitude $\sigma_a = 0$, it follows from Eqs. (6) and (8) that

$$\frac{\Delta\tau_A(\theta)}{2} = |\tau_a \cos 2\theta| \quad \text{and} \quad \sigma_{\perp\max}(\theta) = |\tau_a \sin 2\theta| \quad (14)$$

The Case A shear crack is predicted in the direction with the highest Findley's damage parameter, and therefore $\partial(\cos 2\theta + \alpha_F \cdot \sin 2\theta)/\partial\theta = 0$ results in

$$-\sin 2\theta + \alpha_F \cdot \cos 2\theta = 0 \Rightarrow \theta = \theta_{cr} = 0.5 \cdot \tan^{-1}(\alpha_F) \quad (\text{Case A, pure torsion}) \quad (15)$$

Hence, it is possible to write that under pure cyclic torsion

$$\frac{1}{\sqrt{1 + \alpha_F^2}} + \alpha_F \frac{\alpha_F}{\sqrt{1 + \alpha_F^2}} = \frac{1 + \alpha_F^2}{\sqrt{1 + \alpha_F^2}} = \sqrt{1 + \alpha_F^2} \Rightarrow \tau_a \cdot \sqrt{1 + \alpha_F^2} = \beta_F \quad (\text{Case A, pure torsion}) \quad (16)$$

In the fatigue limit case, the fully-reversed uniaxial Eq. (13) should adopt $\sigma_a = S_L(R = -1)$, while the pure-torsion Eq. (16) would use $\tau_a = \tau_L$, resulting in

$$\begin{cases} S_L \cdot \left(\sqrt{1 + \alpha_F^2} + \alpha_F \right) = 2 \cdot \beta_F \\ \tau_L \cdot \left(\sqrt{1 + \alpha_F^2} \right) = \beta_F \end{cases} \Rightarrow \frac{\sqrt{1 + \alpha_F^2}}{\sqrt{1 + \alpha_F^2} + \alpha_F} = \frac{S_L}{2\tau_L} \Rightarrow \frac{\alpha_F}{\sqrt{1 + \alpha_F^2}} = 2 \cdot \frac{S_L}{\tau_L} - 1 \quad (17)$$

Solving these equations for α_F and β_F , it is found that

$$\alpha_F = \frac{1 - 0.5 \cdot S_L / \tau_L}{\sqrt{S_L / \tau_L - 1}}, \quad \beta_F = \frac{0.5 \cdot S_L}{\sqrt{S_L / \tau_L - 1}} \quad (\text{Findley's calibration for Case A shear}) \quad (18)$$

The above Findley calibration is the most used in the literature, however it is not appropriate if Case B shear cracks initiate. In this case, a similar derivation could be performed for Case B shear cracks, resulting in different calibration parameters

$$\alpha_F = \frac{1 - S_{Lp} / S_L}{S_{Lp} / S_L - 0.5}, \quad \beta_F = \frac{0.5 S_{Lp}}{S_{Lp} / S_L - 0.5} \quad (\text{Findley's calibration for Case B shear}) \quad (19)$$

where S_{Lp} is the pulsating uniaxial fatigue limit measured for $R = 0$. Clearly, the calibration from Eq. (19) is only coherent if pulsating stresses slightly above S_{Lp} would indeed initiate Case B (instead of Case A) shear cracks in the considered material. The calibration values from Eqs. (18) and (19) can be significantly different, therefore they should not be interchangeably used.

It is important to note that the original Findley model does not recognize that its parameters α_F and β_F should have different calibration procedures for calculations to predict the initiation of Case A or Case B shear cracks. Several applications of the Findley model available in the literature implicitly assume initiation of Case A shear cracks in planes perpendicular to the critical point free surface, for which the out-of-plane shear component τ_B is always null. The above proposal to separately calibrate Findley's parameter using Eqs. (18) or (19) has been inspired by McDiarmid's model, which uses separate fatigue limits to independently calibrate its parameters [19,20], recognizing that Case A and Case B shear microcracks should not share the same parameters.

Matake's model [21] is a variation of Findley's criterion that uses the same fatigue damage parameter. However, it oddly searches for the plane of the maximum shear range instead of the plane that maximizes its entire damage parameter to calculate the critical plane direction. Although popular, Matake's model can result in non-conservative predictions if the driving force for fatigue crack initiation is indeed the assumed damage parameter, which is not necessarily maximized at the candidate plane where $\Delta\tau \equiv \Delta\tau_A(\theta)$ is maximum, especially under non-proportional variable amplitude loads. For instance, if the largest shear range only happens for one cycle on a certain plane, while the second largest shear range is repeated over several thousand cycles on a different plane, then it is expected that the plane associated with the second largest is the critical one, and not the maximum shear plane. Therefore, a maximum-damage critical-plane approach needs to be adopted, as opposed to Matake's approach.

For the proportional tension-torsion case with normal and shear amplitudes σ_a and τ_a , Findley's infinite-life equation for Case A candidate planes becomes

$$\max_{\theta} [|\tau_a \cos 2\theta - 0.5 \cdot \sigma_a \cdot \sin 2\theta| + \alpha_F \cdot |\sigma_a \cdot \cos^2 \theta + \tau_a \sin 2\theta|] = \beta_F \quad (20)$$

In the first quadrant $0^\circ \leq \theta \leq 90^\circ$, the right term $\sigma_a \cdot \cos^2 \theta + \tau_a \sin 2\theta$ is never negative (since the amplitudes $\sigma_a \geq 0$ and $\tau_a \geq 0$), however the left term only is positive if $\tan 2\theta < 2\tau_a / \sigma_a = \tan 2\theta_p$, where θ_p is the principal direction from the first quadrant. Therefore, Findley's equation becomes

$$\begin{cases} \max_{\theta} [\tau_a \cos 2\theta - 0.5 \cdot \sigma_a \cdot \sin 2\theta + \alpha_F \cdot \sigma_a \cdot \cos^2 \theta + \alpha_F \cdot \tau_a \sin 2\theta] = \beta_F, & \text{for } 0^\circ \leq \theta \leq \theta_p \\ \max_{\theta} [-\tau_a \cos 2\theta + 0.5 \cdot \sigma_a \cdot \sin 2\theta + \alpha_F \cdot \sigma_a \cdot \cos^2 \theta + \alpha_F \cdot \tau_a \sin 2\theta] = \beta_F, & \text{for } \theta_p < \theta \leq 90^\circ \end{cases} \quad (21)$$

Deriving these expressions and equating them to zero, it can be shown that the critical plane directions θ_F according to Findley's model satisfy

$$\tan 2\theta_F = \frac{2\alpha_F \tau_a \mp \sigma_a}{\alpha_F \sigma_a \pm 2\tau_a} \quad (22)$$

For the entire Case A search space $0^\circ \leq \theta < 180^\circ$, the above expression has four roots, however in general only two of them maximize the damage parameter *globally* along θ , not only *locally*. By replacing θ_F (from the global optimization) into Findley's equation, and after some algebraic manipulation involving the trigonometric relations between $\tan 2\theta_F$, $\sin 2\theta_F$ and $\cos^2 \theta_F$, the infinite-life criterion becomes

$$\sqrt{\sigma_a^2 + 4\tau_a^2} + \frac{\alpha_F}{\sqrt{1 + \alpha_F^2}} \cdot \sigma_a = \frac{2\beta_F}{\sqrt{1 + \alpha_F^2}} \quad (23)$$

This expression helps understand why simplistic invariant-based damage models such as the Crossland's one [22] can give reasonable predictions for metals under simple loadings: if Tresca's factor 4 in Eq. (23) is replaced with von Mises' to give $\sqrt{\sigma_a^2 + 3\tau_a^2} = \Delta\sigma_{\text{Mises}}/2 = \Delta\tau_{\text{Mises}}\sqrt{3}/2$, then it becomes Crossland's criterion

$$\frac{\Delta\tau_{\text{Mises}}}{2} + \alpha_c \cdot (3 \cdot \sigma_{\text{hmax}}) = \beta_c \quad \text{if} \quad \alpha_c \equiv \frac{\alpha_F}{\sqrt{3}\sqrt{1+\alpha_F^2}} \quad \text{and} \quad \beta_c \equiv \frac{2\beta_F}{\sqrt{3}\sqrt{1+\alpha_F^2}} \quad (24)$$

because $\sigma_{\text{hmax}} = \sigma_{\text{max}}/3 = \sigma_a/3$. Crossland's invariant-based criterion might be appropriate for materials that fail due to a distributed mechanism, such as multiple cracking in all directions or microvoid coalescence in cavitation.

However, the use of von Mises and hydrostatic stresses makes this criterion mix fatigue damage from multiple planes, instead of searching for the critical plane where the single dominant crack should initiate, as in most metals. As a result, even though Crossland's model completely misses the physics of crack initiation in most metals, it can approximately reproduce the critical-plane approach predictions for simple in-phase loading. This coincidence makes it evident that more complex non-proportional variable amplitude multiaxial loadings need to be considered to properly evaluate and distinguish such different damage models. In other words, most multiaxial fatigue damage models work well for simple loadings, however this does not mean that they can be used for a more general history, much less for materials different from the ones used in the experimental comparison.

Findley's infinite-life model from Eq. (9) can be extended to finite-life calculations using a shear version of Wöhler's curve, equating Findley's fatigue limit β_F with the torsional fatigue limit τ_L , resulting in

$$\max_{\theta} \left[\frac{\Delta\tau_A(\theta)}{2} + \alpha_F \cdot \sigma_{\perp\text{max}}(\theta) \right] = \frac{\beta_F}{\tau_L} \cdot \tau_c \cdot (2N)^{b_{\tau}} \quad (25)$$

where τ_c and b_{τ} are the torsional strength coefficient and exponent, respectively, calibrated under pure torsion. Note that the above β_F is not equal to τ_L , because Findley's maximum-damage critical-plane approach is adopted in the model calibration; β_F is equal to τ_L only for the case of Matake's maximum shear range calibration. For the studied in-phase tension-torsion history, Findley's predicted fatigue life N_F (in cycles) becomes

$$\sqrt{\sigma_a^2 + 4\tau_a^2} + \frac{\alpha_F}{\sqrt{1+\alpha_F^2}} \cdot \sigma_a = \frac{2\beta_F}{\tau_L\sqrt{1+\alpha_F^2}} \cdot \tau_c \cdot (2N_F)^{b_{\tau}} \quad (26)$$

$$\Rightarrow N_F = 0.5 \cdot \left[\left(\sqrt{1+\alpha_F^2} \cdot \sqrt{\sigma_a^2 + 4\tau_a^2} + \alpha_F \cdot \sigma_a \right) \cdot \frac{\tau_L}{2\beta_F\tau_c} \right]^{1/b_{\tau}} \quad (27)$$

Therefore, N_F can be obtained as a function of σ_a and τ_a , where α_F and β_F are obtained from the normal and shear fatigue limits S_L and τ_L calibrated using the presented Findley's calibration for Case A shear from Eq. (18).

3.3. Smith-Watson-Topper's tensile model

Findley's [3] or Fatemi-Socie's [4] model are not appropriate for tensile-sensitive materials, where Case A tensile cracks initiate. In these materials, the fatigue initiation life N of such cracks must be correlated with a damage parameter based on a normal range $\Delta\varepsilon_{\perp}$ (not on a shear range $\Delta\gamma$), combined with the peak stress $\sigma_{\perp\text{max}}$ parallel to ε_{\perp} to account for mean/maximum stress effects.

The multiaxial version of Smith-Watson-Topper's (SWT) model [5] is particularly useful for calculating fatigue damage of such materials, especially if the propagation phase of the microcracks (still within the so-called crack initiation stage), which is more sensitive to the normal stresses, is dominant over its shear-controlled initiation. The multiaxial version of SWT's equation for Case A tensile cracks can be written as

$$\max_{\theta} \left(\sigma_{\perp\text{max}}(\theta) \cdot \frac{\Delta\varepsilon_{\perp}(\theta)}{2} \right) = \frac{\sigma_c^2}{E} (2N)^{2b} + \sigma_c \varepsilon_c (2N)^{b+c} \quad (28)$$

where σ_c , ε_c , b and c are Coffin-Manson's material parameters.

In high-cycle fatigue calculations, an elastic version of the SWT model, ESWT, can be adopted. Under linear-elastic uniaxial conditions, the plastic term $\sigma_c \varepsilon_c (2N)^{b+c}$ in Eq. (28) can be neglected, while Hooke's law gives $\Delta\sigma_{\perp}(\theta)/2 = E \cdot \Delta\varepsilon_{\perp}(\theta)/2$, resulting in

$$\text{ESWT} = \max_{\theta} \left(\sigma_{\perp\text{max}}(\theta) \cdot \frac{\Delta\sigma_{\perp}(\theta)}{2} \right) = \sigma_c^2 (2N)^{2b} \quad (29)$$

This equation can be simplified in the studied proportional history (which has zero mean stresses), because in this fully-alternate case the peak normal stress $\sigma_{\perp\text{max}}(\theta)$ perpendicular to a Case A plane along θ is equal to the normal amplitude $\Delta\sigma_{\perp}(\theta)/2$. Therefore, the ESWT equation becomes the Wöhler's curve using Basquin's formulation:

$$\max_{\theta} \left(\sigma_{\perp\text{max}}(\theta) \cdot \frac{\Delta\sigma_{\perp}(\theta)}{2} \right) = \max_{\theta} \left[\left(\frac{\Delta\sigma_{\perp}(\theta)}{2} \right)^2 \right] = \sigma_c^2 (2N)^{2b} \Rightarrow \max_{\theta} \left(\frac{\Delta\sigma_{\perp}(\theta)}{2} \right) = \sigma_c (2N)^b \quad (30)$$

Thus, the damage parameter to be maximized in the ESWT model simply becomes $\Delta\sigma_{\perp}(\theta)/2$ for a fully-alternate loading. Deriving Eq. (7) and equating it to zero, the critical plane orientation θ_{ESWT} in the first quadrant $0^{\circ} \leq \theta \leq 90^{\circ}$ is obtained from

$$-\sigma_a \cdot 2 \cos \theta \sin \theta + 2\tau_a \cos 2\theta = 0 \Rightarrow \tan 2\theta_{\text{ESWT}} = \frac{2\tau_a}{\sigma_a} = \tan 2\theta_p = 2 \tan \lambda \quad (31)$$

where λ is the stress amplitude ratio from the SSF model [6], and θ_p is the principal direction from the first quadrant. Not surprisingly, θ_{ESWT} is one of the fixed principal directions θ_p of such proportional tension-torsion loadings. On this principal plane, the damage parameter is maximized, resulting in the principal stress equation for the normal and shear amplitudes σ_a and τ_a :

$$\frac{\Delta\sigma_{\perp}(\theta_{\text{ESWT}})}{2} = \sigma_a \frac{1 + \cos 2\theta_{\text{ESWT}}}{2} + \tau_a \sin 2\theta_{\text{ESWT}} = \frac{\sigma_a + \sqrt{\sigma_a^2 + 4\tau_a^2}}{2} \quad (32)$$

For such an in-phase tension-torsion loading (where both $\sigma_a \geq 0$ and $\tau_a \geq 0$), the other principal direction $\theta_{\text{ESWT}} + 90^{\circ}$ always results in a lower $\Delta\sigma_{\perp}(\theta)/2$, therefore it does not need to be considered. Notice that the maximized damage parameter on the θ_{ESWT} plane can be expressed as a function of σ_a and λ , using the relation $\tau_a = \sigma_a \tan \lambda$, thus:

$$\frac{\Delta\sigma_{\perp}(\theta_{\text{ESWT}})}{2} = \frac{\sigma_a + \sqrt{\sigma_a^2 + 4\sigma_a^2 \tan^2 \lambda}}{2} = \sigma_a \cdot \left[0.5 + \sqrt{0.25 + \tan^2 \lambda} \right] \quad (33)$$

Assuming that the ESWT model is able to predict crack initiation, the above expression would explain why the SSF can be represented as a function of σ_a and λ , however requiring a fifth-order polynomial function to approximately reproduce such a non-linear expression.

Finally, from the ESWT equation it follows that the predicted fatigue life N_{ESWT} (in cycles) is

$$N_{\text{ESWT}} = 0.5 \cdot \left[\frac{\Delta\sigma_{\perp}(\theta_{\text{ESWT}})}{2\sigma_c} \right]^{1/b} = 0.5 \cdot \left[\frac{\sigma_a + \sqrt{\sigma_a^2 + 4\tau_a^2}}{2\sigma_c} \right]^{1/b} = 0.5 \cdot \left[\frac{\sigma_a}{\sigma_c} \cdot \left(0.5 + \sqrt{0.25 + \tan^2 \lambda} \right) \right]^{1/b} \quad (34)$$

4. Materials and methods

4.1. Material

The material used in this work is the DIN 42CrMo4 (AISI 4140) low alloy steel. These metal alloys are heat treated by austenitizing, quenching, and tempering to improve their mechanical properties. This treatment is improved due to the chromium and molybdenum addition, which gives a variety of strength and ductility combinations. This material has been widely used in automotive components such as crankshafts, front vehicle axles, steering components and hot forging components. The chemical composition is given in Table 1.

Specimens used in the fatigue tests series were produced from rods with 25 mm of diameter and its geometry and dimensions reported in [23]. The specimens were inspected and manually polishing through sandpapers of decreasing grit since from 200 to 1200. The monotonic and cyclical properties of 42CrMo4 steel are shown in Table 2.

4.2. Loading paths

Fatigue tests were carried out through a tension/torsion servo-hydraulic fatigue testing machine under stress control at room temperature; the testing frequency was 5 Hz. The six loading paths performed in this study where: alternate tension-compression, alternate torsion, proportional and non-proportional tension/torsion loading. In order to perform the SSF mapping, three different proportional loading paths with three different stress amplitude ratios were selected. One additional case was considered, a non-proportional 90° out of phase loading path, in order to correlate and evaluate the achieved SSF with experimental data. A full description of these study can be found in [6]. For the 42CrMo4 steel used in this study the fatigue material constants for the SSF function described in Equation (1) and (2) determined from the previous described experimental tests, are presented in Table 3.

Table 1
42CrMo4 chemical composition [23].

Element	C	Si	Mn	P	S	Cr	Ni	MO	Cu
Weight (%)	0.39	0.17	0.77	0.025	0.02	1.1	0.3	0.16	0.21

Table 2
42CrMo4 monotonic and cyclic mechanical properties.
[23]

Tensile strength σ_u (MPa)	1100
Cyclic strength coefficient K (MPa)	1420
Yield strength σ_y (MPa)	980
Cyclic strength exponent n' (MPa)	0.12
Elongation ε (%)	16
Fatigue strength coefficient σ_c (MPa)	1154
Young's modulus E (GPa)	206
Fatigue strength exponent b (MPa)	0.061
Hardness (HV)	362
Fatigue ductility coefficient ε_c (MPa)	0.18
Cyclic yield strength (MPa)	640
Fatigue ductility exponent c (MPa)	0.53

Table 3
Coefficients for the SSF function [23].

a	b	c	d	f	g	h	i
2.69	-9.9E-03	1.69E-05	-9.52E-09	-5.99	11.72	-8.04	1.63

5. Results and discussion

The tested 42CrMo4 steel has the monotonic and cyclic elastic and plastic properties presented in Table 2. The ESWT model adopts an elastic version of Coffin–Manson's equation, which neglects its plastic term (thus ignoring ε_c and c). Therefore, the resulting purely-elastic calibration requires a larger σ_c and lower b (in-between the original exponents b and c) to better fit experimental data for lower fatigue lives, see Fig. 2. This figure shows that $\sigma_c = 1654$ MPa and $b = -0.0934$ provide a good fit, assuming as well a normal fatigue limit $S_L = 450$ MPa to account for one run-out experiment beyond $2 \cdot 10^6$ cycles. Fig. 2 also shows the fitting $\tau_c = 911$ MPa and $b_\tau = -0.0623$ of the shear stress-life curve from pure torsion experiments, where the shear fatigue limit τ_L is estimated as 350 MPa. From the normal and shear fittings, it is possible to write:

$$\sigma_a = \sigma_c \cdot (2N)^b = 1654 \cdot (2N)^{-0.0934} \quad \text{and} \quad \tau_a = \tau_c \cdot (2N)^{b_\tau} = 911 \cdot (2N)^{-0.0623} \quad (35)$$

Then, from Findley's calibration for Case A cracks from Eq. (18), the constants are $\alpha_F = 0.668$ and $\beta_F = 420.9$ MPa.

Fig. 3 shows ESWT's damage parameter normalized by the normal fatigue limit S_L , $\Delta\sigma_\perp(\theta)/2S_L$, as a function of the Case A candidate plane angle θ , for the particular in-phase case with amplitudes $\sigma_a = \tau_a = 290$ MPa. From Eqs. (31) and (33), ESWT's

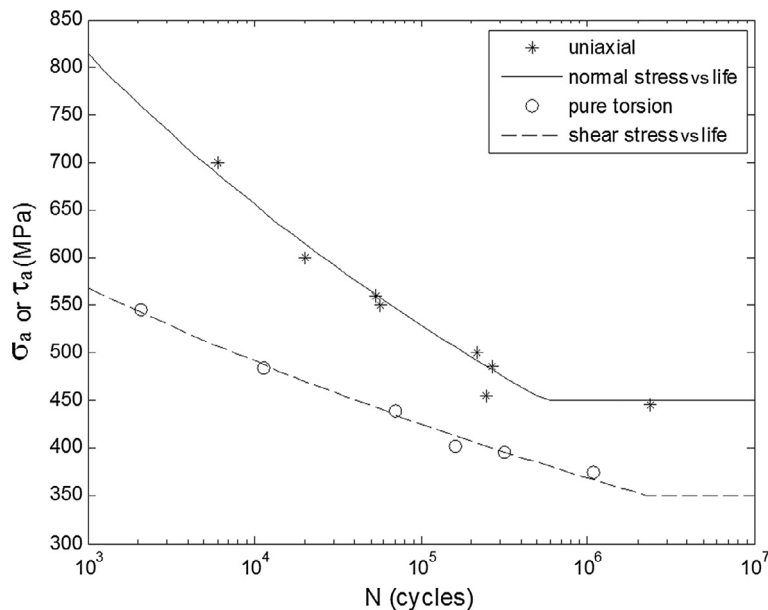


Fig. 2. Fitting of the stress-life curves from the uniaxial and pure torsion experiments.

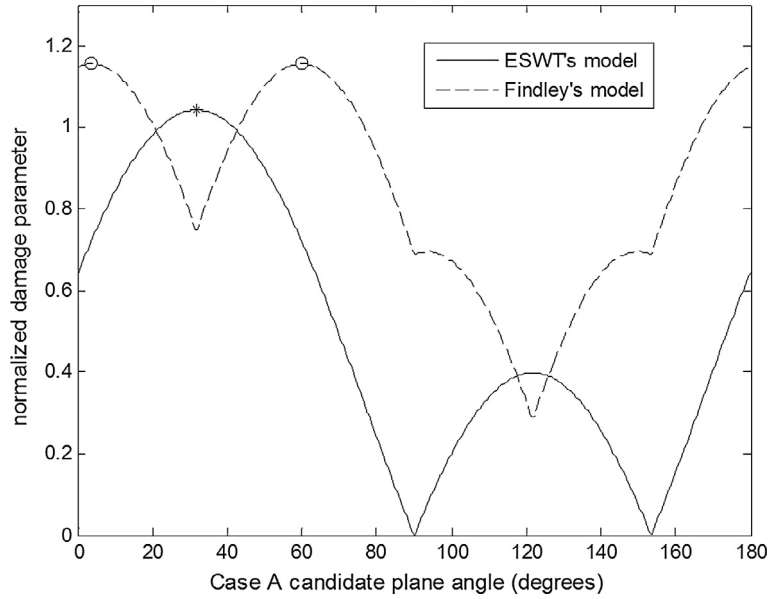


Fig. 3. Normalized damage parameters $\Delta\sigma_{\perp}(\theta)/2S_L$ and $[\Delta\tau_A(\theta)/2 + \alpha_F \cdot \sigma_{\perp\max}(\theta)]/\beta_F$ as a function of the Case A candidate plane angle θ , for an in-phase tension-torsion history with amplitudes $\sigma_a = \tau_a = 290$ MPa.

normalized damage parameter is maximized for $\theta_{\text{ESWT}} = 0.5 \cdot \tan^{-1}(2\tau_a/\sigma_a) \cong 31.7^\circ$, reaching $\Delta\sigma_{\perp}(\theta)/2S_L \cong 1.04$, see Fig. 3. Since this normalized parameter is larger than 1.0, a Case A tensile crack would initiate along this plane characterized by the above value of θ_{ESWT} , according to ESWT's model.

However, Findley's normalized damage parameter, $[\Delta\tau_A(\theta)/2 + \alpha_F \cdot \sigma_{\perp\max}(\theta)]/\beta_F$, reaches a slightly higher maximum, approximately 1.16, calculated from Eqs. (22) and (23) for a critical-plane angle $\theta_F = 0.5 \cdot \tan^{-1}[(2\alpha_F\tau_a - \sigma_a)/(\alpha_F\sigma_a + 2\tau_a)] \cong 3.6^\circ$, as well as for another root of Eq. (22), namely $\theta_F = 0.5 \cdot \tan^{-1}[(2\alpha_F\tau_a + \sigma_a)/(\alpha_F\sigma_a - 2\tau_a)] + 90^\circ \cong 59.8^\circ$, see Fig. 3. Since Findley's model predicts a higher maximum damage than ESWT, the Case A crack should initiate in shear (not tension) in one of the θ_F planes 3.6° or 59.8° . Notice that such planes are associated with Forsyth's stage 1 microcracks [24], during early stages of initiation, not to be mistaken by the direction of Forsyth's stage 2 macroscopic cracks. Such stage 1 plane directions can be difficult to measure in practice, since they involve a very small portion of the resulting macroscopic crack.

For constant amplitude histories, such as the ones in this work, the maximization process can be directly carried out for the damage parameter from the adopted model, as exemplified in Fig. 3. However, under variable amplitude loading, Miner's rule should be applied to rainflow-counted load events from each candidate plane to find its accumulated damage, which would then be maximized for the critical plane.

Figs. 4–6 present a comparison between the observed fatigue lives N_{obsv} and the N_{SSF} , N_{ESWT} and N_F predicted fatigue lives by the SSF, ESWT and Findley's methods, respectively, for stress amplitude ratios $\lambda = 0^\circ$ (uniaxial), 30° , 45° , 60° and 90° (pure torsion). As observed in Fig. 4, the polynomial fitting of the SSF expression is well performed, allowing a good correlation between N_{obsv} and N_{SSF} for all cases.

As shown in Fig. 5, ESWT's critical-plane method results in reasonable fatigue life predictions, except for the pure torsion ($\lambda = 90^\circ$) case. This result suggests that the pure torsion history involved significant shear damage, as expected, however ESWT's model only accounts for tensile damage.

Findley's critical-plane method also results in reasonable fatigue life predictions, except for the $\lambda = 30^\circ$ and $\lambda = 45^\circ$ cases, see Fig. 6. This result suggests that these histories involved significant tensile damage, however Findley's model only accounts for shear damage. The maximum normal stress $\sigma_{\perp\max}$ influences Findley's shear damage parameter, however no measure of the normal range $\Delta\sigma_{\perp}$ perpendicular to the critical plane is considered. Nevertheless, Findley's predictions for the uniaxial case are surprisingly good, indicating that the $\sigma_{\perp\max}$ term was able to capture the damaging $\Delta\sigma_{\perp}$ effects.

Fig. 7 shows critical-plane predictions based on ESWT's tensile model applied to the predominantly tensile cases $\lambda = 0^\circ$ (uniaxial), 30° , and 45° , and on Findley's shear model to the shear-dominated cases $\lambda = 60^\circ$ and 90° (pure torsion). Notice that the prediction scatter is not too different from the one obtained by means of the SSF method shown in Fig. 4. However, such critical-plane method calculations have a greater prediction potential, because they are only based on curve fittings of the uniaxial and pure torsion experiments from Fig. 2, while the polynomial from the SSF method requires data from all five tests to be properly calibrated. Alternatively, a more conservative version of Fig. 7 can have been generated from the minimum life between the predicted N_{ESWT} and N_F for each experiment, as usually assumed for the critical-plane approach by using separate tensile and shear-based damage models.

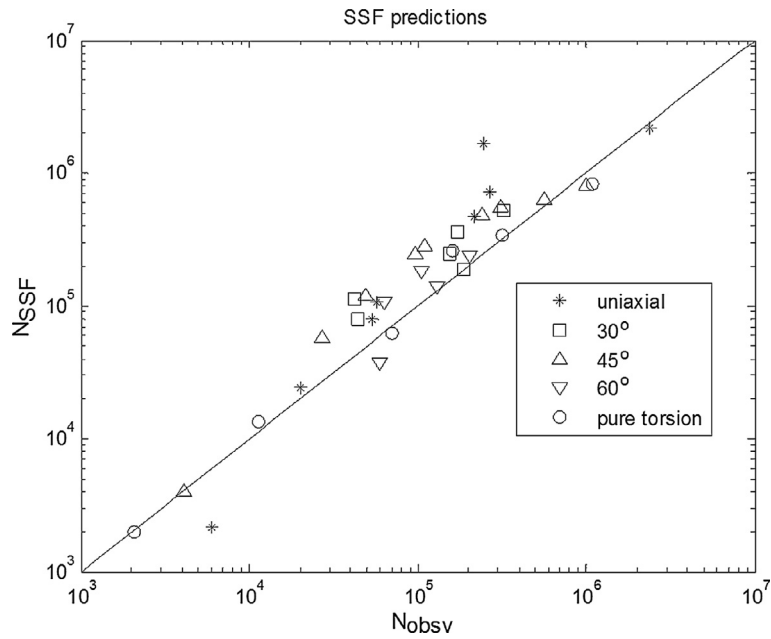


Fig. 4. Comparison between the observed fatigue lives N_{obsv} and the N_{SSF} predicted by the SSF method.

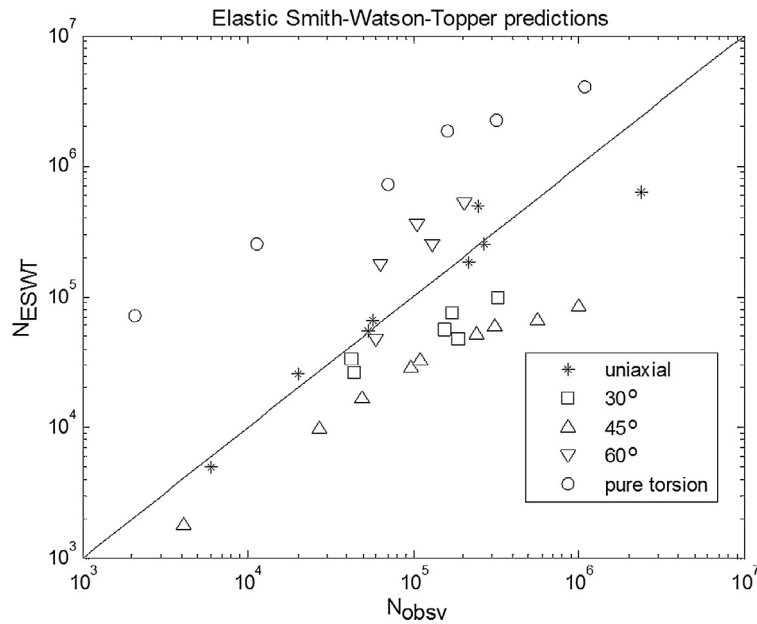


Fig. 5. Comparison between the observed fatigue lives N_{obsv} and the N_{ESWT} predicted by the ESWT critical-plane method.

6. Conclusions

In this work, it has been shown that both critical-plane and stress scale factors (SSF) approaches have the potential to predict multiaxial fatigue lives, at least for in-phase proportional loadings. SSF approach reveals a much better prediction lives than the critical plane approaches used. In particular Findley's model neglects tensile damage, while the Elastic Smith, Watson and Topper (ESWT) model neglects shear damage, which explains why their performance was not very good for all considered load histories. Perhaps, other critical-plane models that mix shear and tensile damage, such as Susmel's [25–27] and Papuga's [28], might provide better overall fatigue life estimates for a wider range of load history types. It has been also shown that Findley's model for in-phase tension-torsion histories results in a Tresca version of the von-Mises-invariant-

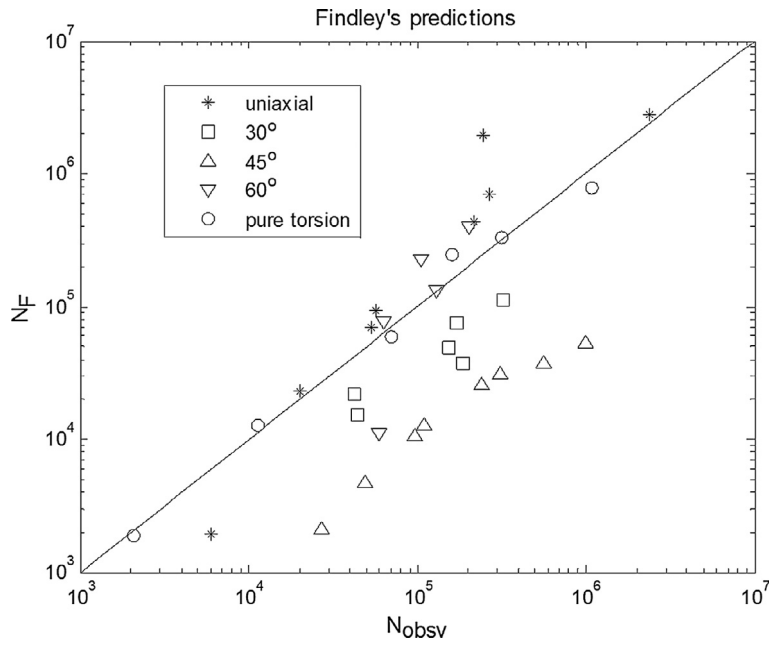


Fig. 6. Comparison between the observed fatigue lives N_{obsv} and the N_F predicted by Findley's critical-plane method.

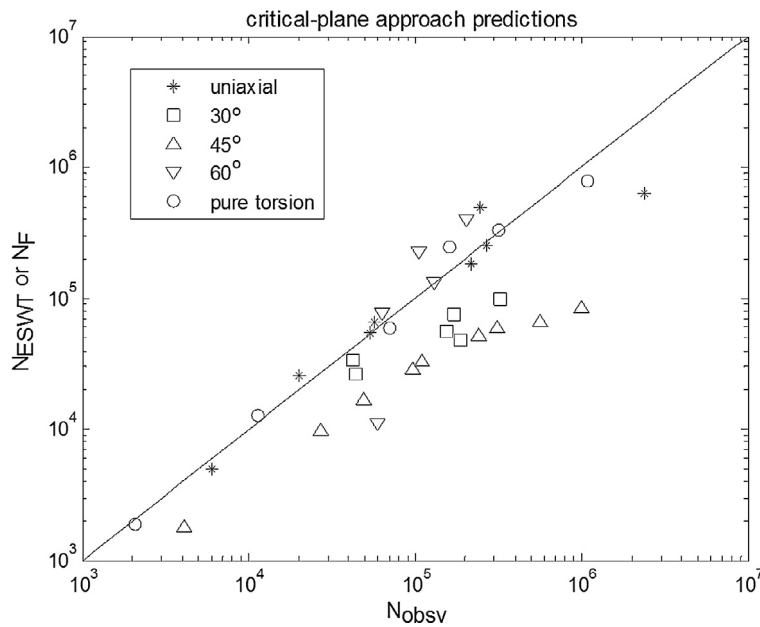


Fig. 7. Comparison between the observed fatigue lives N_{obsv} and the N_{ESWT} or N_F predicted by ESWT's or Findley's critical-plane methods, depending on the dominance of normal or shear applied loads.

based model from Crossland, which helps to explain why several multiaxial damage models can provide good predictions for simple loadings, even though they might completely miss the physics of the problem. In its current form, the SSF method does not include mean/maximum stress effects, therefore experiments with zero mean loads were chosen to evaluate its performance. The SSF method resulted in a better fit of the experimental data than the critical plane approach, however it requires more calibration tests (to fit its fifth-degree polynomial).

References

- [1] Socie DF, Marquis GB. *Multiaxial fatigue*. SAE International; 2000.
- [2] Castro JTP, Meggiolaro MA. *Fatigue design techniques* (in 3 volumes). Scotts Valley (CA, USA): CreateSpace; 2016.
- [3] Findley WN. A theory for the effect of mean stress on fatigue of metals under combined torsion and axial load or bending. *J Eng Ind* 1959;81:301–6.
- [4] Fatemi A, Socie D. A critical plane approach to multiaxial damage including out-of-phase loading. *Fatigue Fract Eng Mater Struct* 1988;11:149–66.
- [5] Smith RN, Watson P, Topper TH. A stress-strain parameter for the fatigue of metals. *J Mater* 1970;5:767–78.
- [6] Anes V, Reis L, Li B, Fonte M, de Freitas M. New approach for analysis of complex multiaxial loading paths. *Int J Fatigue* 2014;62:21–33.
- [7] Anes V, Reis L, Li B, Freitas M. New cycle counting method for multiaxial fatigue. *Int J Fatigue* 2014;67:78–94.
- [8] Anes V, Reis L, Li B, Freitas M, Sonsino CM. Minimum circumscribed ellipse (MCE) and stress scale factor (SSF) criteria for multiaxial fatigue life assessment. *Theoret Appl Fract Mech* 2014;73:109–19.
- [9] Araújo JA, Carpinteri A, Ronchei C, Spagnoli A, Vantadori S. An alternative definition of the shear stress amplitude based on the Maximum Rectangular Hull method and application to the C-S (Carpinteri-Spagnoli) criterion. *Fatigue Fract Eng Mater Struct* 2014;37(7):764–71.
- [10] Carpinteri A, Ronchei C, Spagnoli A, Vantadori S. Lifetime estimation in the low/medium-cycle regime using the Carpinteri-Spagnoli multiaxial fatigue criterion. *Theoret Appl Fract Mech* 2014;73:120–7.
- [11] Lopez-Crespo P, Moreno B, Lopez-Moreno A, Zapatero J. Study of crack orientation and fatigue life prediction in biaxial fatigue with critical plane models. *Eng Fract Mech* 2015;136:115–30.
- [12] Mohammadi M, Zehsaz M, Hassanifard S, Rahmatfam A. An evaluation of total fatigue life prediction of a notched shaft subjected to cyclic bending load. *Eng Fract Mech* 2016;166:128–38.
- [13] Lagoda T, Macha E, Nieslony A. Fatigue life calculation by means of the cycle counting and spectral methods under multiaxial random loading. *Fatigue Fract Eng Mater Struct* 2005;28(4):409–20.
- [14] Carpinteri A, Spagnoli A, Vantadori S. Fatigue life estimation under multiaxial random loading using a critical plane-based criterion. In: *Proceedings of the 2nd international conference on material and component performance under variable amplitude loading*, Darmstadt, Germania, vol. 1, p. 475–84.
- [15] Carpinteri A, Spagnoli A, Ronchei C, Scorza D, Vantadori S. Critical plane criterion for fatigue life calculation: time and frequency domain formulations. *Procedia Eng* 2015;101:518–23.
- [16] Karolczuk A, Macha E. Selection of the critical plane orientation in two-parameter multiaxial fatigue failure criterion under combined bending and torsion. *Eng Fract Mech* 2008;75:389–403.
- [17] Carpinteri A, Ronchei C, Scorza D, Vantadori S. Critical plane orientation influence on multiaxial high-cycle fatigue assessment. *Phys Mesomech* 2015;18(4):348–54.
- [18] Bannantine JA, Socie DF. A variable amplitude multiaxial fatigue life prediction method. In: *Fatigue under biaxial and multiaxial loading*, 10. ESIS Publ; 1991. p. 35–51.
- [19] McDiarmid DL. A general criterion for high cycle multiaxial fatigue failure. *Fatigue Fract Eng Mater Struct* 1991;14:429–53.
- [20] McDiarmid DL. A shear stress based critical-plane criterion of multiaxial fatigue failure for design and life prediction. *Fatigue Fract Eng Mater Struct* 1994;17:1475–84.
- [21] Mataka T. An explanation on fatigue limit under combined stress. *Bull Jpn Soc Mech Eng* 1977;20:257–63.
- [22] Crossland B. Effect of large hydrostatic pressures on the torsional fatigue strength of an alloy steel. In: *Int conf fatigue metals*. London: IMechE; 1956. p. 138–49.
- [23] de Freitas M, Reis L, Li B. Comparative study on biaxial low-cycle fatigue behaviour of three structural steels. *Fatigue Fract Eng Mater Struct* 2006;29:992–9.
- [24] Forsyth PJE. *The physical basis of metal fatigue*. Blackie and Son; 1969.
- [25] Susmel L, Lazzarin P. A bi-parametric Wöhler curve for high cycle multiaxial fatigue assessment. *Fatigue Fract Eng Mater Struct* 2002;25:63–78.
- [26] Susmel L. Multiaxial fatigue limits and material sensitivity to non-zero mean stresses normal to the critical planes. *Fatigue Fract Eng Mater Struct* 2008;31:295–309.
- [27] Susmel L. On the overall accuracy of the modified Wöhler curve method in estimating high-cycle multiaxial fatigue strength. *Frattura ed Integrità Strutturale* 2011;16:5–17.
- [28] Papuga J, Ruzicka M. Two new multiaxial criteria for high cycle fatigue computation. *Int J Fatigue* 2008;30:58–66.